RSC Advances

PAPER

View Article Online
View Journal | View Issue

Cite this: *RSC Adv.*, 2024, **14**, 20130

Morpholine-modified Ru-based agents with multiple antibacterial mechanisms as metalloantibiotic candidates against *Staphylococcus aureus* infection†

Shijie Lin,‡[a] Yun Song,‡[b] Yajuan Sun,‡[b] Wenjing Lin,[b] Guangying Yu,[b] Xiangwen Liao [b] and Qiang Yang [*c]

Multidrug-resistant bacteria resulting from the abuse and overuse of antibiotics have become a huge crisis in global public health security. Therefore, it is urgently needed to develop new antibacterial drugs with unique mechanisms of action. As a versatile moiety, morpholine has been widely employed to enhance the potency of numerous bioactive molecules. In this study, a series of ruthenium-based antibacterial agents modified with the morpholine moiety were designed and characterized, aiming to obtain a promising metalloantibiotic with a multitarget mechanism. Antibacterial activity screening demonstrated that the most active complex **Ru(II)-3** exhibited the strongest potency against *Staphylococcus aureus* (*S. aureus*) with an MIC value of only 0.78 μg mL^{-1}, which is better than most clinically used antibiotics. Notably, **Ru(II)-3** not only possessed excellent bactericidal efficacy, but could also overcome bacterial resistance. Importantly, **Ru(II)-3** very efficiently removed biofilms produced by bacteria, inhibited the secretion of bacterial exotoxins, and enhanced the activity of many existing antibiotics. The results of mechanism studies confirmed that **Ru(II)-3** could destroy the bacterial membrane and induce ROS production in bacteria. Furthermore, animal infection models confirmed that **Ru(II)-3** showed significant anti-infective activity *in vivo*. Overall, this work demonstrated that a morpholine-modified ruthenium-based agent is a promising antibiotic candidate in tackling the crisis of drug-resistant bacteria.

Received 9th April 2024
Accepted 6th June 2024

DOI: 10.1039/d4ra02667e

rsc.li/rsc-advances

1. Introduction

Nowadays, multidrug-resistant bacteria pose a huge threat to global health, with an increasing number of people losing their lives every year. Among them, *Staphylococcus aureus* (*S. aureus*) is one of the most common Gram-positive bacteria, causing a variety of infections, such as joint infection, skin infection, and bacteremia, ranging from sub-acute superficial skin infection to life-threatening septicemia.[1–4] It has been reported that the notorious "superbug", methicillin-resistant *S. aureus* (MRSA), resulted in more than 100 000 deaths and 3.5 million disabilities in 2019.[5,6] Moreover, the outbreak of COVID-19 (coronavirus disease) has triggered a massive use of antibiotics, further increasing antimicrobial resistance and worsening the problem.[7,8] Therefore, it is urgently needed to develop novel antibacterial drugs, especially those with unique mechanisms of action, to combat antibiotic-resistant bacteria.

As a representative transition metal, ruthenium (Ru) has aroused great interest because of its excellent biological activity. Its rich photophysical and chemical properties are very suitable for drug development. Moreover, the similarity in the action of ruthenium to that of iron not only reduces the toxicity of Ru-based drugs, but also endows it with different oxidation states in different physiological states.[9–11] These advantages make Ru-based agents modified with a bioactive moiety exhibit robust antibacterial efficacy and effectively prevent bacteria from developing resistance.[12–16]

Morpholine is a natural six-membered ring, which has been widely exploited to enhance the potency of numerous bioactive molecules because of its superior physicochemical, biochemical, and metabolic properties.[17] It was reported that the weakly basic N in morpholine could enhance solubility, whereas the oxygen atom forms hydrogen bonding, which enhances its potency against the target protein by establishing hydrophobic interactions.[18] Notably, morpholine-modified agents exhibited

[a]*Department of Pharmacy, Hainan General Hospital (Hainan Affiliated Hospital of Hainan Medical University), Haikou, 570311, China*

[b]*Jiangxi Provincial Key Laboratory of Drug Design and Evaluation, School of Pharmacy, Jiangxi Science & Technology Normal University, Nanchang, 330013, China*

[c]*Department of Clinical Pharmacy, Hainan Cancer Hospital, Haikou, 570100, China. E-mail: 18789551643@163.com*

† Electronic supplementary information (ESI) available. See DOI: https://doi.org/10.1039/d4ra02667e

‡ These authors contribute equally to this work.

a wide range of biological properties, including anti-inflammatory, antioxidant, antibacterial, and antitumor activities.[19,20] In various antibiotics, the morpholine moiety also has an important effect on their antibacterial activity (Scheme 1A).[17]

Herein, in order to screen a promising metalloantibiotic with a multitarget mechanism and robust potency, we introduced a morpholine moiety into an Ru-based structure and then obtained a series of novel Ru-based antibacterial agents (Scheme 1B). Subsequently, their antibacterial activity against *S. aureus* was studied *in vitro*. Then, the most effective agent, **Ru(II)-3**, was selected for the antibacterial mechanism study. Furthermore, the ability of **Ru(II)-3** to clear bacterial biofilms was confirmed,

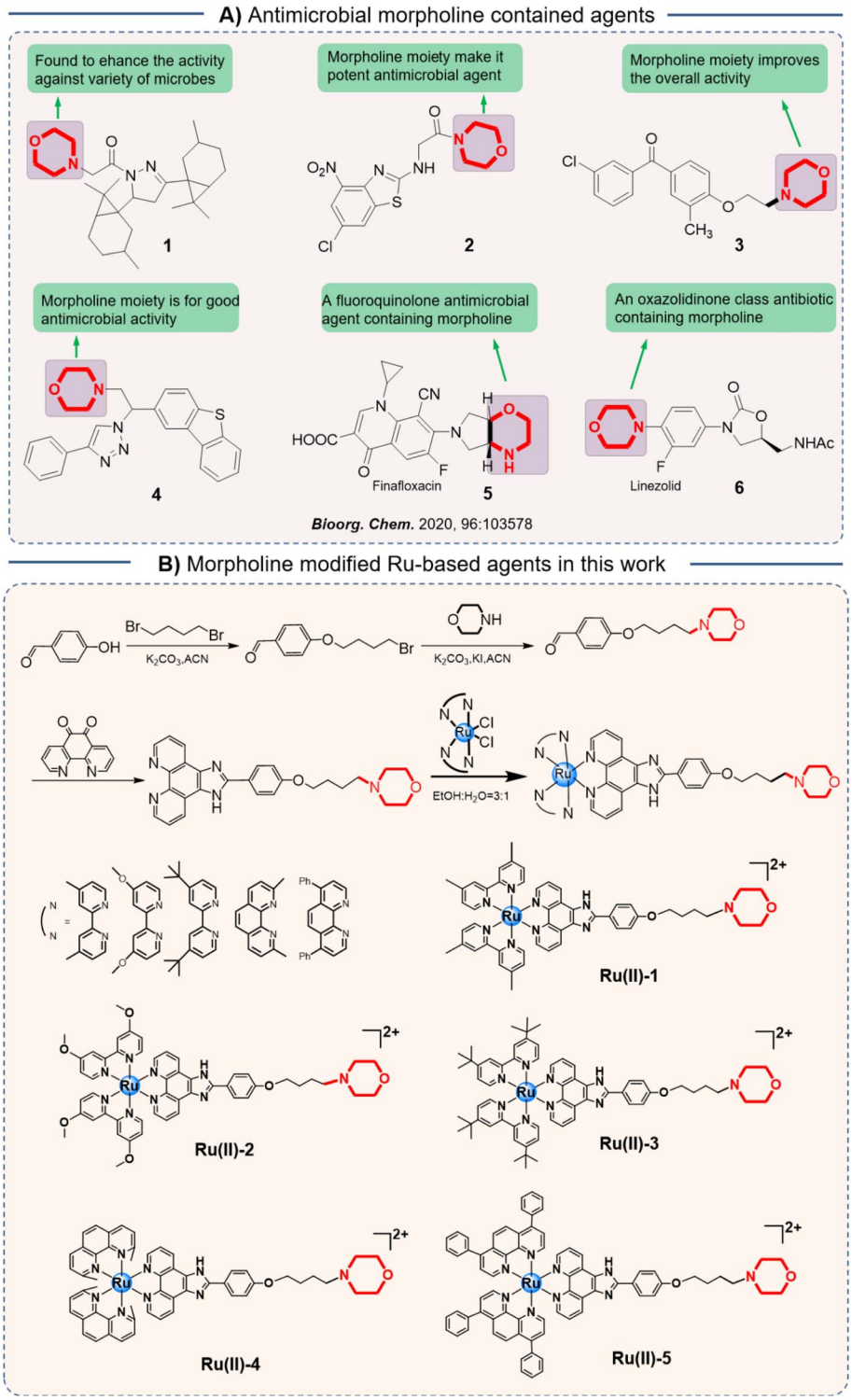

Scheme 1 (A) Antimicrobial morpholine contained agtents reported before; (B) the design of five Ru-based agents modified with morpholine and their synthesis routes.

which may help overcome bacterial resistance. Notably, the anti-toxin efficacy and synergistic activity of **Ru(II)-3** with existing antibiotics were explored, too. At last, its toxicity and anti-infective potency *in vivo* were verified using animal infection models.

2. Results and discussion

2.1 Antibacterial activity of morpholine-modified Ru-based agents

The morpholine moiety was linked to the Ru-based structure *via* long-chain alkyl groups and the detailed synthesis routes are shown in Scheme 1B. All the complexes were characterized by ^{1}H-NMR, ^{13}C-NMR and HRMS spectroscopy. In addition, their purity was confirmed by HPLC (ESI†). The characterization data are presented in the ESI.† To begin, the minimum inhibitory concentration (MIC) values of five compounds against *S. aureus* were explored and the data are shown in Fig. 1. Five morpholine-modified ruthenium complexes showed good antibacterial activity against *S. aureus*, with the MIC values ranging from 0.78 to 25 μg mL^{-1}. Importantly, the best candidate agent, namely, **Ru(II)-3**, exhibited the strongest antibacterial effect, and has an MIC value of only 0.78 μg mL^{-1}. This potency is much better than most clinically common antibiotics, too (Fig. 1). In addition, **Ru(II)-3** also exhibited robust effectiveness against drug-resistant MRSA isolated from the clinic (Table S1†). Furthermore, the rapid bactericidal efficacy, a feature that helps in efficiently controlling acute bacterial infections, of **Ru(II)-3** was investigated through a time–kill curve analysis. Notably, **Ru(II)-3** killed more than 99% of bacteria in just 2 h at 0.78 μg mL^{-1}. When the concentration was increased to 1.56 μg mL^{-1}, the time required was only 1 h (Fig. 2). At last, the antibacterial effect of five agents on *S. aureus* was directly monitored through a bacterial growth curve. As exhibited in Fig. 3, the growth of *S. aureus* was completely inhibited by the five tested agents at the MIC. Collectively, these data suggest that these morpholine-modified Ru-based agents possess robust antibacterial potency *in vitro*.

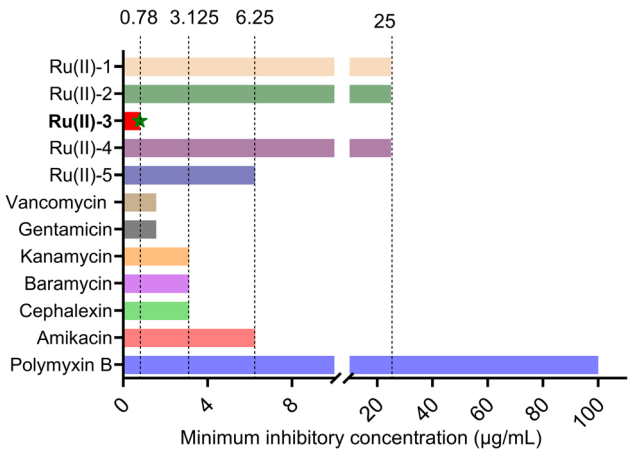

Fig. 1 MIC values of five ruthenium complexes and some clinical antibiotics against *S. aureus*.

2.2 Evaluating the frequencies of drug resistance

The main reason why bacterial infections have become increasingly difficult to deal with is that bacteria can easily develop resistance to antibiotics because of which clinicians are left with few weapons to deal with such multidrug-resistant bacteria. Hence, novel antibacterial drugs with unique mechanisms of action, for which it is difficult for bacteria to develop resistance, are urgently needed. Therefore, in order to verify whether complex **Ru(II)-3** can overcome bacterial resistance, a resistance development assay was employed.[21] As shown in Fig. 4, after continuously exposing to ciprofloxacin (0.5 MIC) for 20 generations, *S. aureus* developed significant resistance since the MIC of ciprofloxacin against it increased by 64 times. However, under the same condition, the MIC values of **Ru(II)-3** against *S. aureus* only increased by 4 times, suggesting that **Ru(II)-3** could not easily produce drug resistance in *S. aureus*.

2.3 Inhibition of hemolytic toxin secretion

It has been reported that the exotoxin of *S. aureus* is essential for it to spread through tissues and survive under host

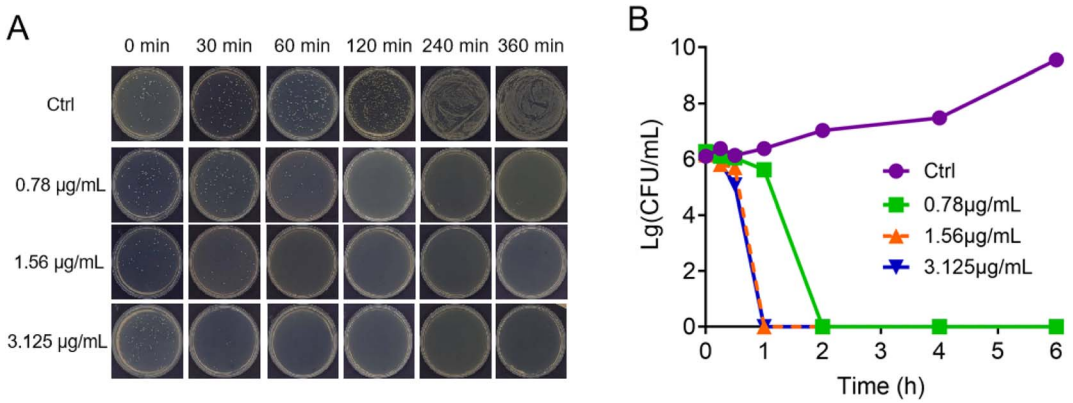

Fig. 2 Bactericidal effect of **Ru(II)-3** against *S. aureus* at different concentrations after 6 h (A). Time–kill curve of **Ru(II)-3** against *S. aureus* (B); *S. aureus* without **Ru(II)-3** is the negative control.

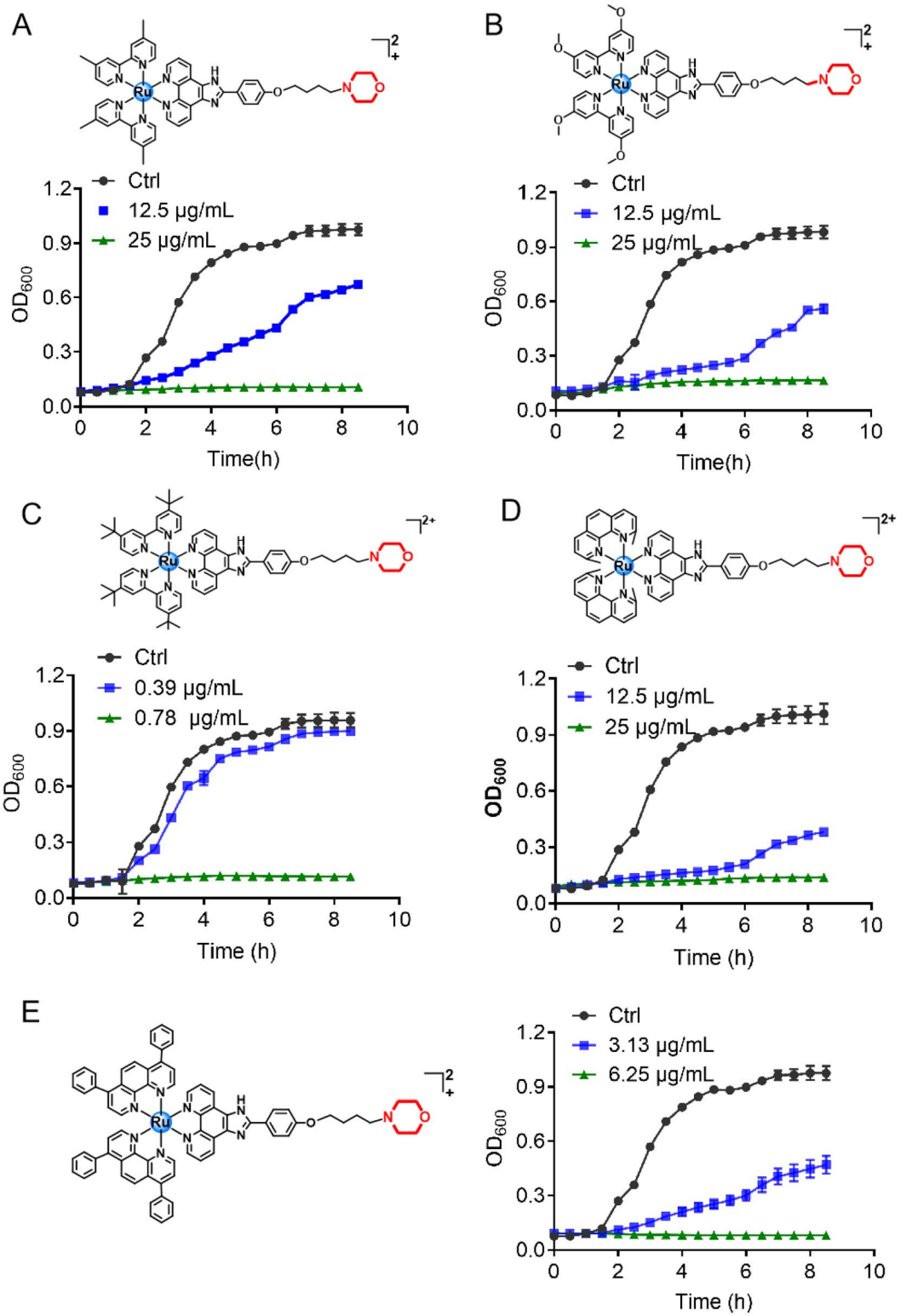

Fig. 3 Growth curve of *S. aureus* in the presence of Ru-based compounds. (A) **Ru(II)-1**; (B) **Ru(II)-2**; (C) **Ru(II)-3**; (D) **Ru(II)-4**; (E) **Ru(II)-5**.

immune-cell clearance. Therefore, the ability of antibacterial agents to inhibit the secretion of toxins is very beneficial for them to remove bacteria *in vivo* more effectively.[22] Here, in order to further study the inhibitory effect of **Ru(II)-3** on the secretion of α-toxin from *S. aureus*, a hemolysis test using rabbit blood cells was performed. In brief, *S. aureus* was co-incubated with a sub-inhibitory concentration of **Ru(II)-3**; then, the bacterial supernatant was collected and incubated

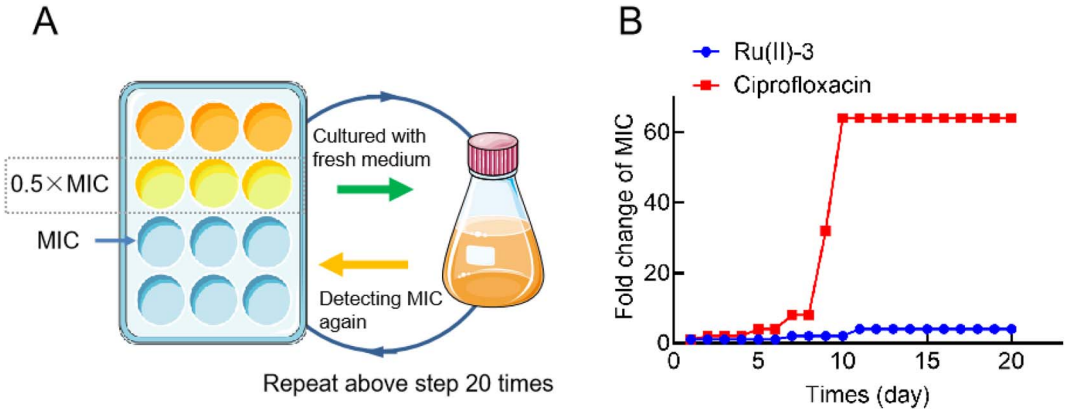

Fig. 4 Illustration of resistance development assay (A). Changes in minimum inhibitory concentration (MIC) over time against *S. aureus* exposed to sub-inhibitory concentrations of **Ru(II)-3** or ciprofloxacin for 20 days (B).

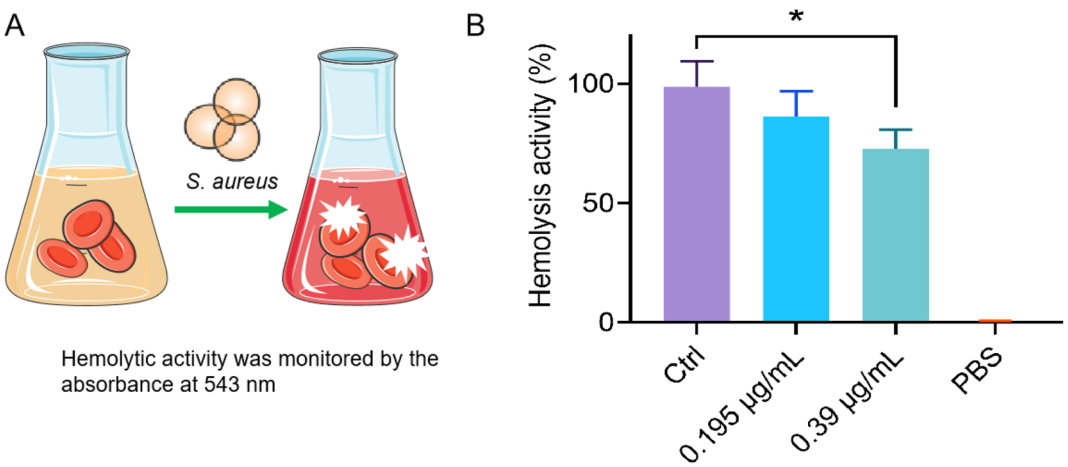

Fig. 5 Hemolysis test using rabbit blood cells (A); hemolytic toxin activity of *S. aureus* supernatants after incubation with 0.195 or 0.39 μg mL^{-1} of **Ru(II)-3** (B). All the experiments were performed with three biological replicates. The statistical difference is determined through two-tailed Student's *t*-test. Only significant differences are annotated: $*P < 0.05$, $**P < 0.01$, $***P < 0.001$, and $****P < 0.0001$.

with rabbit blood at 37 °C for 30 min. As shown in Fig. 5, after co-incubating with **Ru(II)-3**, the hemolytic effect of the bacterial supernatant on blood cells was obviously broken, indicating that **Ru(II)-3** effectively inhibited α-toxin production from *S. aureus*. It is noteworthy that **Ru(II)-3** itself did not obviously destroy red blood cells even at 250 μg mL^{-1} (Fig. S29†), suggesting its good biocompatibility.

2.4 Biofilm inhibition by Ru(II)-3

As a defense barrier, the formation of a biofilm greatly promotes the resistance of bacteria to antibiotics; therefore, the effective removal of bacterial biofilms urgently needs to be addressed. Consequently, the anti-biofilm potency of **Ru(II)-3** was explored. To begin, *S. aureus* was co-incubated with the sub-inhibitory concentration of **Ru(II)-3** at 37 °C for 48 h, and then the formation of a biofilm was monitored using a crystal violet staining assay. As shown in Fig. 6A, only at 0.195 μg mL^{-1} (0.25 MIC), **Ru(II)-3** remarkably prevented the formation of a biofilm in *S. aureus*, with an inhibition rate above 90%. Next, the destructive effect of **Ru(II)-3** on the already formed biofilm was investigated. The data presented in Fig. 6B clearly indicate that more than 50% of the mature biofilm was eradicated in the presence of 0.39 μg mL^{-1} **Ru(II)-3** (0.5 MIC). Taken together, these results presented here demonstrated that **Ru(II)-3** could efficiently inhibit bacterial biofilm formation. More importantly, it also has a powerful ability to remove mature biofilms. Of course, this ability of **Ru(II)-3** might also explain, to some extent, why *S. aureus* could not easily develop resistance to it.

2.5 Synergistic activity of Ru(II)-3 with antibiotics

In recent years, the development of antimicrobial adjuvants—agents that can increase the antibiotic potency and even reverse drug resistance—has been an alternative approach to combat antibiotic-resistant bacteria.[23] In order to investigate the synergistic activity of **Ru(II)-3** with antibiotics, the checkerboard

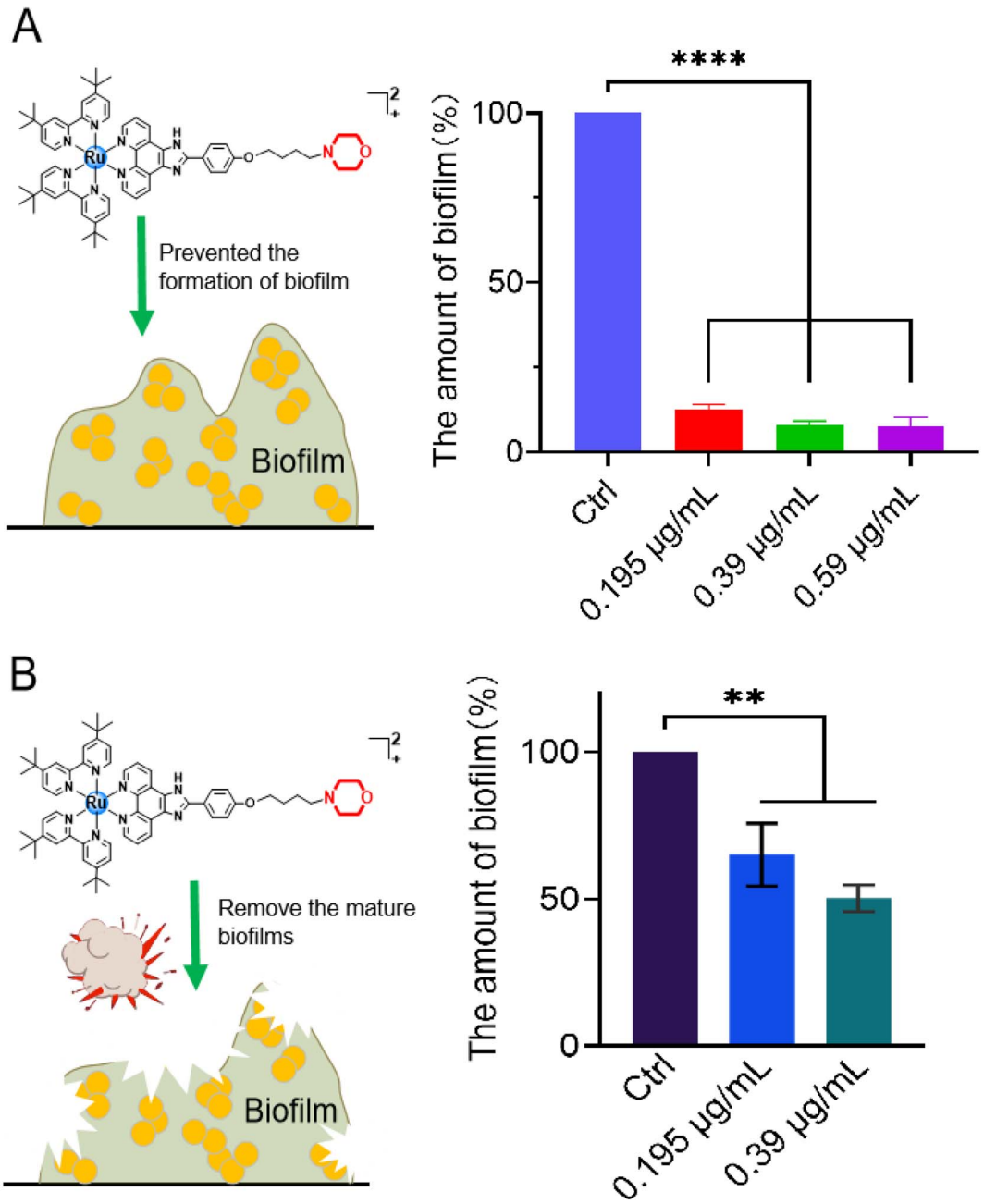

Fig. 6 (A) Formation of *S. aureus* biofilm inhibited by **Ru(II)-3** at different concentrations; the amount of biofilm quantified by the absorbance at 595 nm after staining with crystal violet; (B) eradication effect on a mature biofilm of **Ru(II)-3** was monitored by detecting the number of viable bacteria in the matured biofilm. All the experiments were performed with three biological replicates. All the data are shown as mean ± sd. The statistical difference is determined using two-tailed Student's *t*-test. Only significant differences are annotated: $*P < 0.05$, $**P < 0.01$, $***P < 0.001$, and $****P < 0.0001$.

method was employed. At first, nine clinically used antibiotics from different categories were selected. Then heat-map data were drawn and the corresponding fractional inhibitory concentration index (FICI; a value of ≤0.5 suggests synergism) was calculated when a combination of these antibiotics was used with **Ru(II)-3** against *S. aureus*. As shown in Fig. 7, **Ru(II)-3** significantly enhanced the antibacterial efficacy of two antibiotics against *S. aureus*, namely, ampicillin (FICI, 0.31) and polymyxin B (FICI, 0.5), suggesting that **Ru(II)-3** could effectively enhance the antibacterial activity of some clinically used antibiotics.

2.6 Antibacterial mechanism exploration

The advantage of Ru-based agents is that they exhibit multi-target actions, such as bacterial membrane destruction and reactive oxygen species (ROS) induction, an antimicrobial

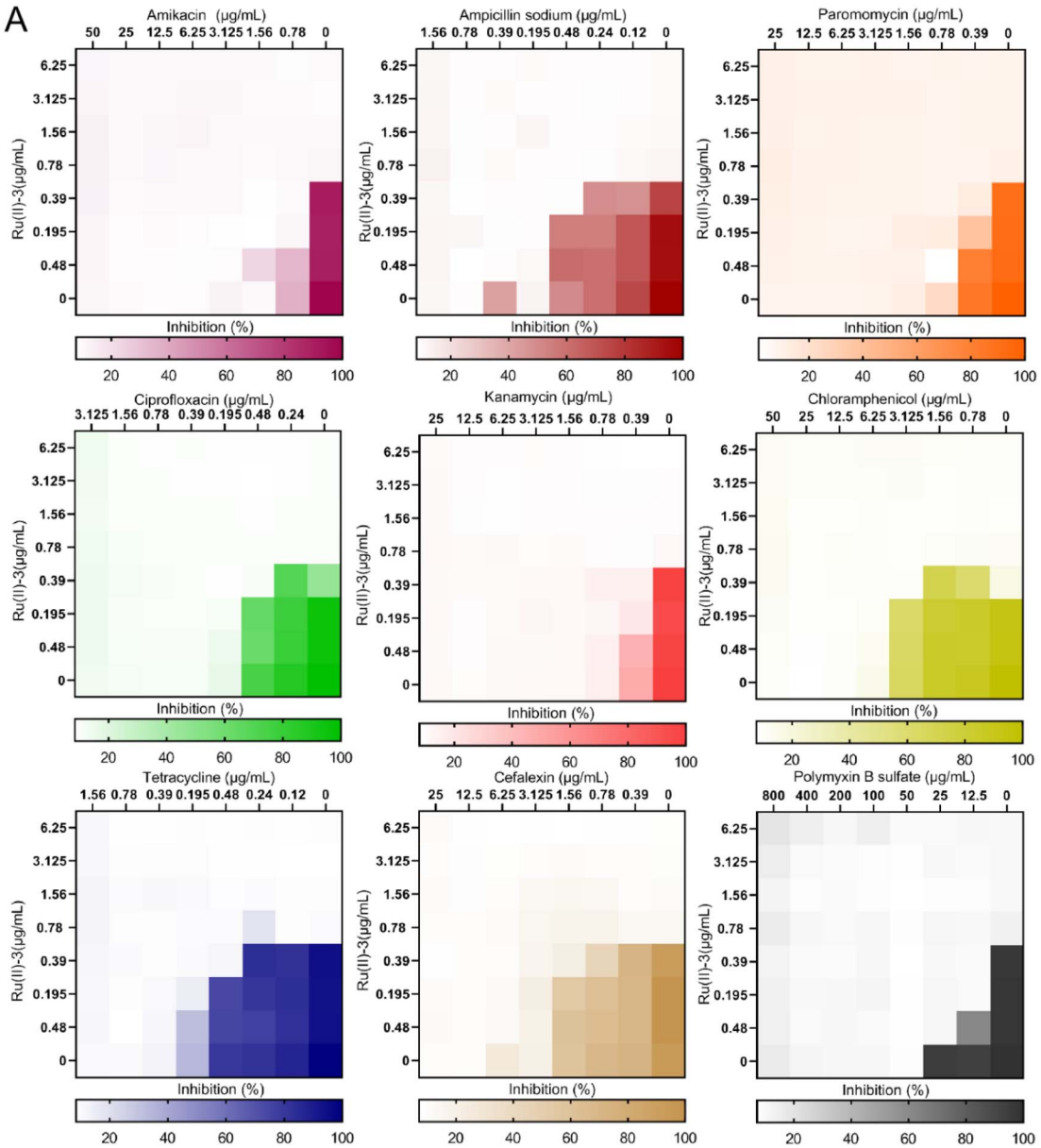

B

Antibiotic	MIC (μg/mL)	FICI
Paromomycin	1.56	0.625
Ciprofloxacin	0.195	1
Tetracycline	0.39	0.75
Cefalexin	12.5	0.625
Ampicillin sodium	0.78	**0.3125**
Amikacin	1.56	0.75
Kanamycin	0.78	0.75
Chloramphenicol	6.25	1
Polymyxin B sulfate	50	**0..5**

Fig. 7 Heat maps of the checkerboard assays (A) and the corresponding fractional inhibitory concentration indices (FICI) values (B) when **Ru(II)-3** combination was used with nine antibiotics against *S. aureus*. An isobologram analysis of the synergistic effects of **Ru(II)-3** with ampicillin and polymyxin B sulfate (C).

mechanism different from that of traditional antibiotics.[16] Therefore, the destruction effect of **Ru(II)-3** on the bacterial membrane was first verified by measuring the leakage of nucleic acid. As shown in Fig. 8A, after incubation with **Ru(II)-3** or polymyxin B for 2 h, the nucleic acid leakage from *S. aureus* increased by 40% and 49%, respectively, indicating a breakdown of the bacterial cell membrane. It has been reported that the breakage of the bacterial membrane can lead to its depolarization.[24] Therefore, 3,3′-dipropylthiadicarbocyanine iodide [$DiSC_3(5)$], a dye for depolarization monitoring, was employed to further explore the effect of **Ru(II)-3** on the bacterial membrane potential. As shown in Fig. 8B, a strong green fluorescence appeared when *S. aureus* was incubated with **Ru(II)-3** for 2 h, indicating the membrane depolarization. Next, PI and DAPI, two common fluorescence probes for bacterial-cell staining,[25] were employed to further monitor the damage effect of **Ru(II)-3** on the bacterial membrane. Normally, if some bacteria showed red fluorescence, it indicates that their cell

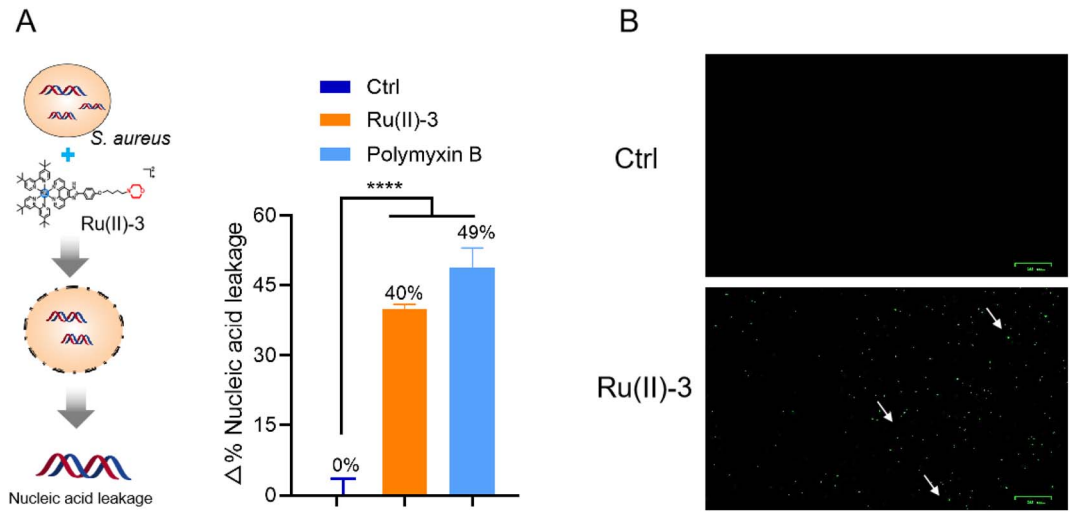

Fig. 8 Percentage of leaked nucleic acid from bacteria after treatment with **Ru(II)-3** or polymyxin B sulfate at 1 MIC (A); membrane depolarization of *S. aureus* was monitored by $DiSC_3(5)$ dye after treatment with 0.78 μg mL^{-1} **Ru(II)-3** (B). All the images are 25 μm in scale. All the experiments were performed with three biological replicates. The statistical difference is determined using two-tailed Student's *t*-test. Only significant differences are annotated: $^*P < 0.05$, $^{**}P < 0.01$, $^{***}P < 0.001$, and $^{****}P < 0.0001$.

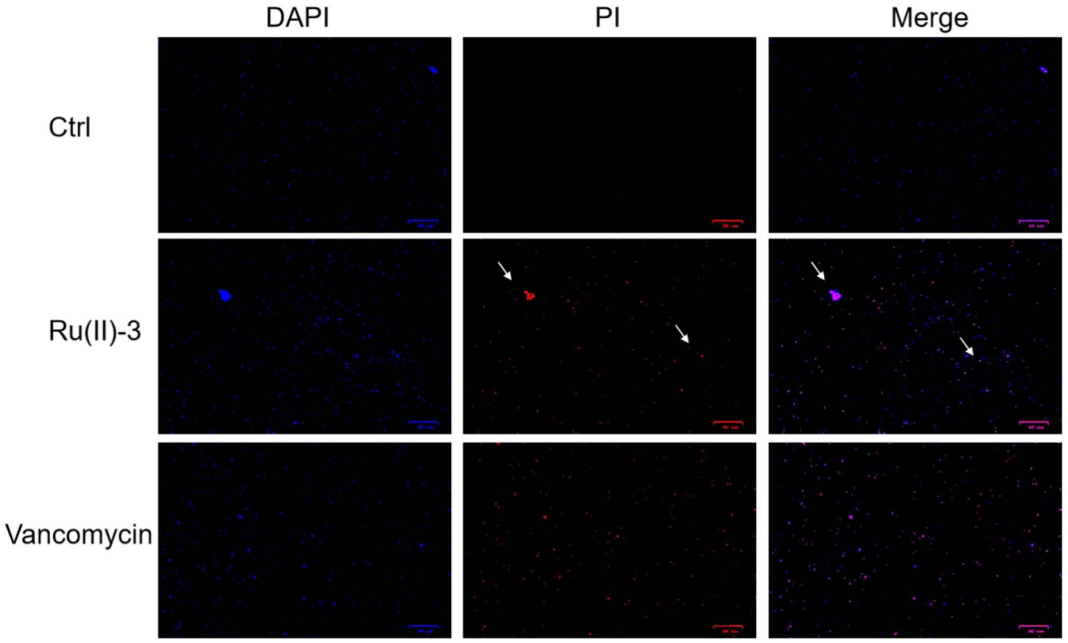

Fig. 9 DAPI and PI staining results of *S. aureus* after treatment with PBS, **Ru(II)-3** or vancomycin at 1 MIC. All the images are 25 μm in scale.

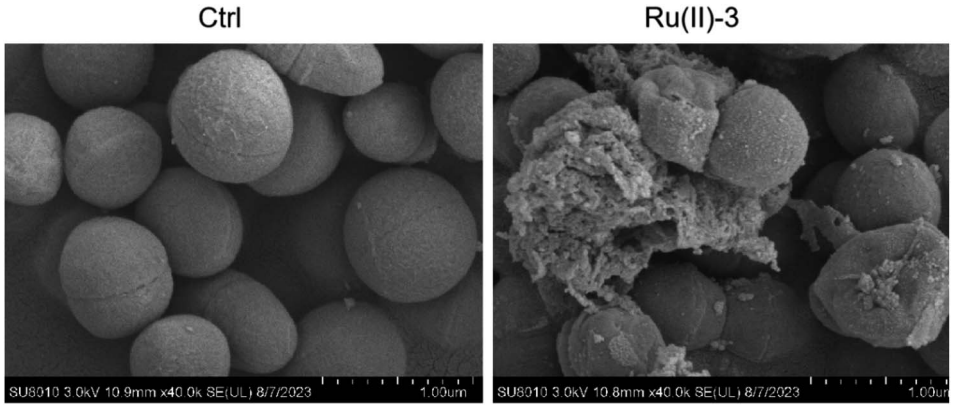

Fig. 10 Scanning electron microscopy (SEM) images of *S. aureus* after treatment with 0.78 μg mL^{-1} **Ru(II)-3**.

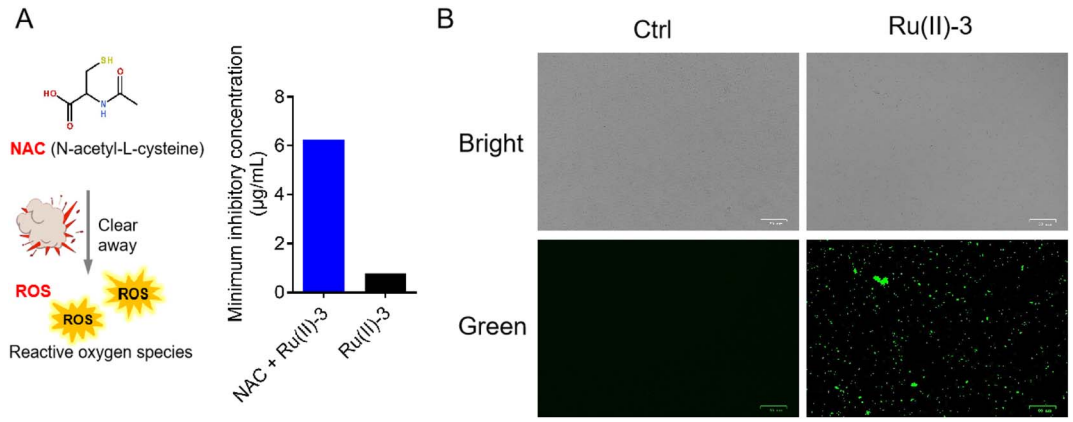

Fig. 11 (A) MIC of **Ru(II)-3** against *S. aureus* in the presence and absence of NAC. (B) Intracellular ROS production in bacteria was detected *via* DCFH-DA after treatment with 1.56 μg mL^{-1} **Ru(II)-3** and photographed using a fluorescence microscope.

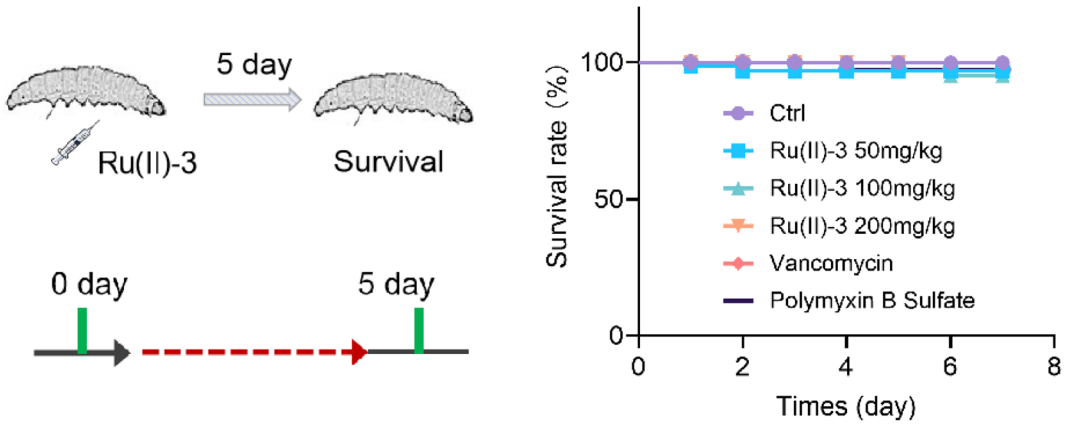

Fig. 12 Toxicity of **Ru(ii)-3** *in vivo*. The survival rate of *G. mellonella* wax worms treated with a high dose of **Ru(II)-3**, vancomycin, or polymyxin B.

membrane is damaged. As shown in Fig. 9, after treatment with **Ru(II)-3** for 2 h, it could be clearly observed that some bacteria were stained with red fluorescence in the presence of two dyes. Notably, a similar phenomenon was also observed in the vancomycin-treated group. This result indicated that **Ru(II)-3** could destroy the integrity of bacterial membranes. Finally, the membrane destruction effect of **Ru(II)-3** was further visually detected by a scanning electron microscope (SEM). As shown in

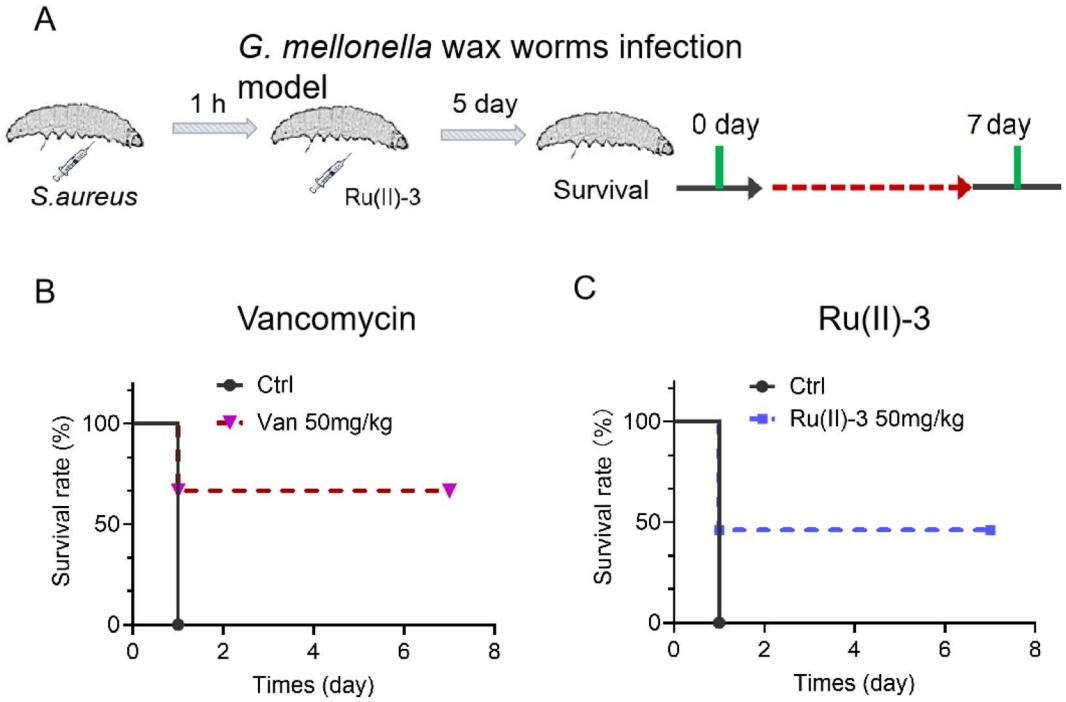

Fig. 13 (A) Scheme of the *G. mellonella* larva infection model. The survival rate of *S. aureus*-infected *G. mellonella* wax worms after treatment with **Ru(II)-3** (C) or vancomycin (B).

Fig. 10, the surface of *S. aureus* in the PBS-treated group was complete and smooth. However, after treatment with **Ru(II)-3**, some bacteria were seriously ruptured. Collectively, these results clearly suggested that **Ru(II)-3** could cause the destruction of the bacterial membrane, thereby achieving the bactericidal effect.

Apart from membrane destruction, ROS production is also one of the most important ways for some Ru-based antibacterial agents to kill bacteria.[16] Next, to further confirm the involvement of ROS in the bactericidal process of **Ru(II)-3**, we evaluated the ROS production in *S. aureus* using two probes, namely, *N*-acetyl-cysteine (NAC) and 2,7-dichlorodihydrofluorescein diacetate (DCFH-DA). Notably, NAC is an ROS scavenger, whereas DCFH-DA is a green fluorescent probe for intracellular ROS.[26] First, the effect of NAC on the antibacterial efficacy of **Ru(II)-3** against *S. aureus* was investigated. As shown in Fig. 11A, the MIC value of **Ru(II)-3** increased by eight times in the presence of ROS scavenger (NAC), suggesting that the clearance of ROS reduced its bactericidal efficacy. Second, the generation of ROS in bacteria was visualized using DCFH-DA.[27] As shown in Fig. 11B, no green fluorescent signals were detected in the PBS-treated group. However, after co-incubation with **Ru(II)-3**, lots of green fluorescent signals were observed in *S. aureus*, indicating the generation of ROS. Taken together, it could be concluded that **Ru(II)-3** mainly killed bacteria in two ways: induce ROS formation and damage the bacterial membrane.

2.7 Antibacterial efficacy *in vivo*

At last, given that **Ru(II)-3** showed excellent antibacterial potency *in vitro*, we further explored its ant-infective efficacy *in vivo*. First, the toxicity of **Ru(II)-3** was verified using *Galleria mellonella* (*G. mellonella*) larva. In brief, *G. mellonella* was injected with a high dose of **Ru(II)-3** and their survival rate was recorded within 7 days. The results demonstrated that complex **Ru(II)-3** has pretty low toxicity *in vivo*, similar to two clinically used antibiotics, vancomycin and polymyxin B. As shown in Fig. 12, even though the injected dose of **Ru(II)-3** reached 200 mg kg^{-1}, above 90% of *G. mellonella* survived.

Next, two animal infection models using *G. mellonella* larva and mouse were employed to investigate the anti-infective potency of **Ru(II)-3**. For the *G. mellonella* infection model,[28] *S. aureus* was injected into them and then treated with **Ru(II)-3** or vancomycin after 1 h. As shown in Fig. 13, all the *S. aureus*-infected *G. mellonella* died on the second day. However, the survival rate of the infected *G. mellonella* after treatment with **Ru(II)-3** was significantly elevated. At a dose of 50 mg kg^{-1}, above 50% *G. mellonella* survived, suggesting the high anti-infective efficacy of **Ru(II)-3**. Next, a mouse wound infection model[29] was established to further verify its antibacterial activity *in vivo*. The schematic of the wound infection model is exhibited in Fig. 14A. The photograph of the mouse wound and changes in size clearly demonstrated that a sterile cream containing **Ru(II)-3** has a good therapeutic effect. At a dose of 100 mg kg^{-1}, **Ru(II)-3** showed stronger anti-infective potency than vancomycin, resulting in a faster wound-healing rate. The size of the mouse wounds in the **Ru(II)-3**-treated group on the 10th day was significantly smaller than that of the vancomycin-treated group (Fig. 14B and C). Importantly, the weight of the mouse did not change significantly throughout the treatment, indicating the low toxicity of **Ru(II)-3** to mice (Fig. 14D).

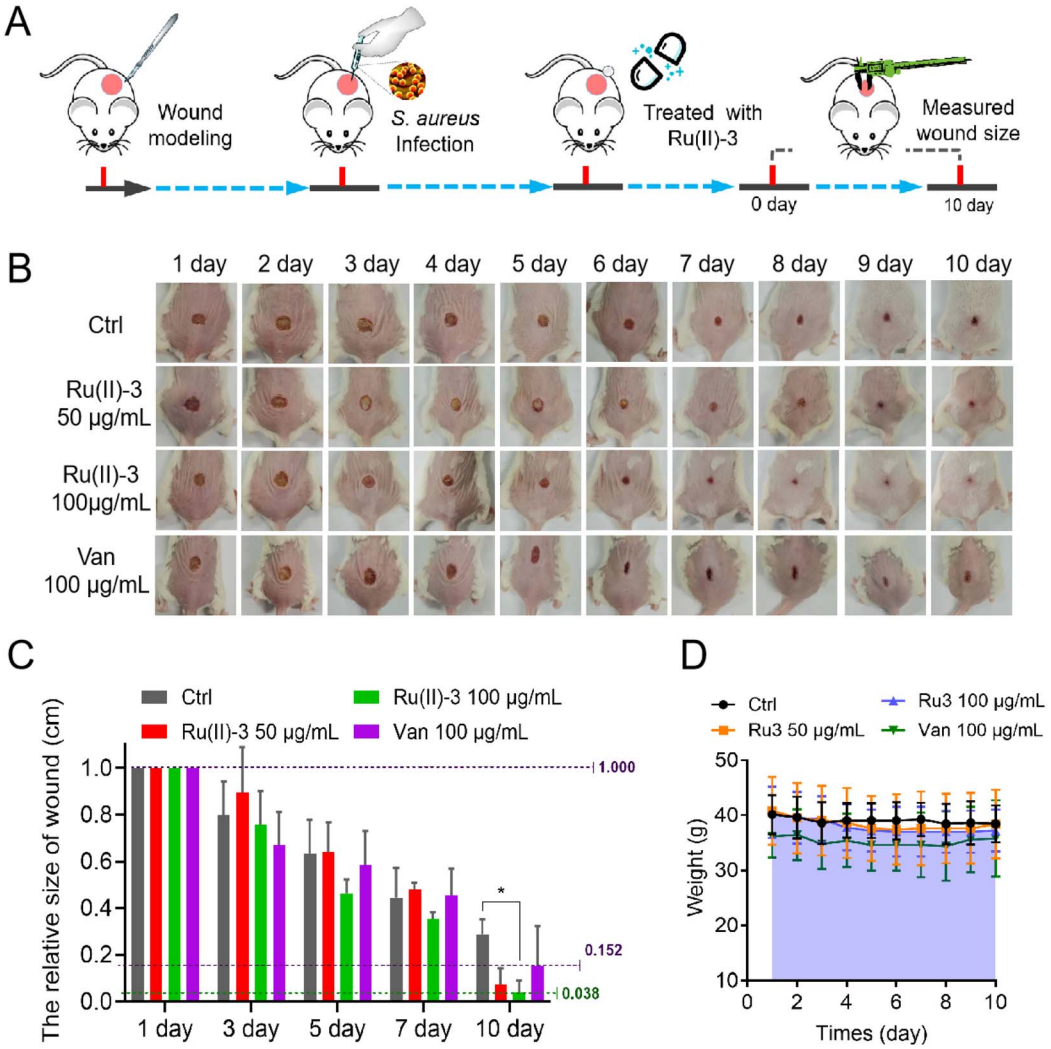

Fig. 14 (A) Scheme of *S. aureus*-infected dermal wound model. (B) Representative photographs of the wounds after treatment with **Ru(II)-3**. (C) Relative size changes of wounds within 10 days. (D) Relative weight changes in mouse within 10 days. Data are shown as mean ± sd and $n = 5$. The statistical difference is determined using two-tailed Student's *t*-test. Only significant differences are annotated: $^{*}P < 0.05$, $^{**}P < 0.01$, $^{***}P < 0.001$, and $^{****}P < 0.0001$.

Collectively, these results confirm that **Ru(II)-3** not only exhibited low toxicity but also had a strong anti-infection effect on *S. aureus in vivo*.

3. Conclusion

In summary, a versatile morpholine moiety was linked into an Ru-based skeleton and then successfully developed into five novel Ru-based antibacterial agents with multiple antibacterial mechanisms in this work. The *in vitro* antibacterial potency evaluation confirmed that all the five agents showed robust bactericidal activity against *S. aureus*. In particular, the most-active agent, **Ru(II)-3**, could kill more than 99% *S. aureus* in just 2 h at 0.78 μg mL^{-1}. In addition, it could effectively inhibit the α-toxin secretion from *S. aureus*. More importantly, **Ru(II)-3** could not only efficiently inhibit bacterial biofilm formation but also had a powerful ability to remove mature biofilms. These properties will help it to remove bacteria more effectively *in vivo*. In fact, **Ru(II)-3** could effectively enhance the antibacterial activity of most traditional antibiotics when a combination was employed. Antibacterial mechanism studies further demonstrated that **Ru(II)-3** exhibited multitarget action: it killed bacteria in mainly two ways: induce ROS formation and damage the bacterial membrane. Due to this series of advantages, **Ru(II)-3** not only showed much better bactericidal potency than most clinically common antibiotics but also efficiently prevented *S. aureus* from achieving drug resistance. At last, two animal infection models also demonstrated that **Ru(II)-3** showed significant efficacy against *S. aureus in vivo* and with low toxicity. Taken together, the results presented here clearly demonstrated that a morpholine-modified ruthenium-based agent is a promising antibiotics candidate in tackling the crisis of drug-resistant bacteria.

4. Experimental section

4.1 Synthesis and characterization

4.1.1 Synthesis of MPLP. A mixture of 4-[4-(morpholin-4-yl) butoxy]benzaldehyde (263.3 mg, 1 mmol), 1,10-phenanthroline-5,6-dione (231.2 mg, 1.1 mmol), ammonium acetate (1541.7 mg, 20 mmol), and acetic acid (15 mL) were refluxed at 85 °C for 10 h. After cooling to room temperature, the mixture was adjusted to neutral with ammonia and then filtered to obtain a crude product. Then, it was recrystallized with ethanol and dried to obtain a brownish yellow product. Yield: 372.9 mg, 82.2%. ^{1}H NMR (400 MHz, DMSO-d_6) δ 13.61 (s, 1H), 9.02 (d, J = 2.8 Hz, 2H), 8.91 (d, J = 8.0 Hz, 2H), 8.21 (d, J = 8.7 Hz, 2H), 7.88–7.79 (m, 2H), 7.16 (d, J = 8.7 Hz, 2H), 4.08 (t, J = 6.2 Hz, 2H), 3.57 (d, J = 4.1 Hz, 4H), 2.44–2.24 (m, 6H), 1.82–1.71 (m, 2H), 1.65–1.54 (m, 2H). ^{13}C NMR (101 MHz, DMSO-d_6) δ 160.37 (s), 151.25 (s), 148.08 (s), 143.97 (s), 136.16 (s), 129.96 (s), 128.29 (s), 126.59 (s), 123.94 (d, J = 56.6 Hz), 122.98 (s), 119.79 (s), 115.39 (s), 68.05 (s), 66.71 (s), 58.25 (s), 53.79 (s), 27.04 (s), 22.85 (s). HRMS (ESI) m/z: calcd for $C_{27}H_{27}N_5O_2$ $[M + H]^+$, 454.2243; found 454.2230.

4.1.2 Synthesis of [Ru(dmb)$_2$(MPLP)](PF$_6$)$_2$ (Ru(II)-1). A mixture containing MPLP (136.0 mg, 0.3 mmol) and $[Ru(dmb)_2Cl_2]\cdot 2H_2O$ (162.1 mg, 0.3 mmol) in ethylene glycol (10 mL) were heated at 150 °C for 8 h under argon. After cooling to room temperature, saturated KPF_6 aqueous solution (15 mL) was added to obtain a dark red precipitate. The crude product is obtained by centrifugation, and is dried and purified by column chromatography (neutral alumina, acetonitrile/xylene = 3 : 1 v/v). Dark red product. Yield: 196.02 mg, 54.0%. ^{1}H NMR (400 MHz, DMSO-d_6) δ 14.16 (s, 1H), 9.05 (d, J = 11.2 Hz, 2H), 8.71 (d, J = 16.2 Hz, 4H), 8.24 (d, J = 6.8 Hz, 2H), 8.05 (s, 2H), 7.91 (s, 2H), 7.66 (s, 2H), 7.42 (s, 4H), 7.29–7.12 (m, 4H), 4.12 (s, 2H), 3.57 (s, 4H), 2.55 (s, 8H), 2.45 (s, 4H), 2.38 (s, 6H), 1.81 (s, 2H), 1.63 (s, 2H). ^{13}C NMR (101 MHz, DMSO-d_6) δ 160.95 (s), 156.74 (d, J = 14.5 Hz), 153.35 (s), 150.94 (d, J = 15.6 Hz), 149.98 (d, J = 14.3 Hz), 137.36 (s), 130.49 (s), 128.98–128.11 (m), 127.73 (s), 126.71 (s), 126.48 (s), 125.96 (s), 125.46 (d, J = 6.1 Hz), 122.34 (s), 121.60 (s), 115.65 (s), 80.06–74.15 (m), 80.06–70.32 (m), 69.17 (d, J = 211.6 Hz), 66.21 (dd, J = 595.2, 425.0 Hz), 58.22 (s), 55.80 (d, J = 450.6 Hz), 29.45 (s), 26.91 (s), 21.15 (d, J = 9.5 Hz). IR (KBr): ν = 3383, 2932, 2860, 2324, 2167, 1978, 1742, 1618, 1553, 1501, 1455, 1383, 1265, 1102, 1030, 841, 553 cm^{-1}. HRMS (ESI): m/z: calcd for $[M - 2PF_6]^{2+}$ $C_{51}H_{51}N_9O_2Ru$, 461.6611; found: 461.6613.

4.1.3 Synthesis of [Ru(dmob)$_2$(MPLP)](PF$_6$)$_2$ (Ru(II)-3). This complex was synthesized in an identical route to that of **Ru(II)-1** only with $[Ru(dmob)_2Cl_2]\cdot 2H_2O$ in place of $[Ru(dmb)_2Cl_2]\cdot 2H_2O$. Dark red product. Yield: 171.2 mg, 44.7%. ^{1}H NMR (400 MHz, DMSO-d_6) δ 14.16 (s, 1H), 9.03 (d, J = 8.0 Hz, 2H), 8.48 (d, J = 18.6 Hz, 4H), 8.24 (d, J = 8.2 Hz, 2H), 8.14 (d, J = 4.4 Hz, 2H), 7.91 (s, 2H), 7.64 (d, J = 6.3 Hz, 2H), 7.29 (d, J = 6.2 Hz, 2H), 7.22 (s, 4H), 6.92 (d, J = 4.8 Hz, 2H), 4.12 (s, 2H), 4.03 (s, 6H), 3.92 (s, 6H), 3.57 (s, 4H), 2.35 (s, 4H), 1.79 (s, 2H), 1.61 (s, 2H).· ^{13}C NMR (101 MHz, DMSO-d_6) δ 166.98 (d, J = 16.4 Hz), 158.38 (d, J = 3.1 Hz), 152.32 (d, J = 16.7 Hz), 150.30 (s), 129.90 (s), 128.72 (s), 127.09 (d, J = 121.4 Hz), 115.65 (s), 114.53 (d, J = 18.8 Hz), 111.76 (s), 68.11 (s), 66.34 (s), 57.98 (s), 57.19 (d, J = 9.6 Hz), 53.52 (s), 40.71 (s), 40.63–40.02 (m), 40.09 (s), 39.98 (d, J = 21.0 Hz), 39.56 (d, J = 21.0 Hz), 39.17–38.36 (m), 26.91 (s), 22.51 (s). IR (KBr): ν = 2959, 2923, 2852, 1617, 1556, 1495, 1465, 1409, 1328, 1312, 1241, 1220, 1104, 1028, 844, 743, 728, 555 cm^{-1}. HRMS (ESI): m/z: calcd for $[M - 2PF_6]^{2+}$ $C_{51}H_{51}N_9O_6Ru$, 493.6510; found: 493.6510.

4.1.4 Synthesis of [Ru(dtbpy)$_2$(MPLP)](PF$_6$)$_2$ (Ru(II)-3). This complex was synthesized in an identical route to that of **Ru(II)-1** with $[Ru(dtbpy)_2Cl_2]\cdot 2H_2O$ in place of $[Ru(dmb)_2Cl_2]\cdot 2H_2O$. Dark red product. Yield: 234.1 mg, 56.5%. ^{1}H NMR (400 MHz, DMSO-d_6) δ 14.19 (s, 1H), 9.07 (d, J = 9.1 Hz, 2H), 8.88 (d, J = 13.4 Hz, 4H), 8.26 (d, J = 8.5 Hz, 2H), 8.04–7.90 (m, 4H), 7.64 (dd, J = 18.2, 5.8 Hz, 4H), 7.46 (t, J = 5.0 Hz, 2H), 7.37–7.29 (m, 2H), 7.23 (d, J = 8.7 Hz, 2H), 4.13 (s, 4H), 3.58 (s, 2H), 1.81 (s, 2H), 1.42 (s, 18H), 1.34 (s, 18H), 1.28 (s, 2H), 1.23 (s, 2H), 0.87 (s, 4H). ^{13}C NMR (101 MHz, DMSO-d_6) δ 162.27 (d, J = 17.8 Hz), 160.68 (s), 157.00 (d, J = 16.8 Hz), 154.51 (s), 151.17 (s), 149.46 (s), 145.27 (s), 130.49 (s), 128.67 (s), 126.44 (s), 125.28 (s), 124.96 (s), 124.13 (s), 123.28 (s), 122.22 (s), 115.50 (s), 67.44 (d, J = 142.1 Hz), 66.44–66.03 (m), 58.27 (s), 53.81 (s), 35.92 (d, J = 13.3 Hz), 30.52 (d, J = 11.2 Hz), 27.04 (s), 22.86 (s), 17.95 (s). IR (KBr): ν = 2954, 2918, 2852, 1612, 1470, 1459, 1465, 1404, 1358, 1241, 1180, 1114, 1069, 1028, 839, 743, 713, 590, 555 cm^{-1}. HRMS (ESI): m/z: calcd for $[M - 2PF_6]^{2+}$ $C_{63}H_{75}N_9O_2Ru$, 545.7552; found: 545.7552.

4.1.5 Synthesis of [Ru(dmp)$_2$(MPLP)](PF$_6$)$_2$ (Ru(II)-4). This complex was synthesized in an identical route to that of **Ru(II)-1** with $[Ru(dmp)_2Cl_2]\cdot 2H_2O$ in place of $[Ru(dmb)_2Cl_2]\cdot 2H_2O$. Dark red product. Yield: 191.8 mg, 50.7%. ^{1}H NMR (400 MHz, DMSO-d_6) δ 14.11 (s, 1H), 8.89 (dd, J = 27.4, 8.1 Hz, 4H), 8.44 (t, J = 8.5 Hz, 4H), 8.25 (d, J = 8.6 Hz, 2H), 8.17 (d, J = 8.3 Hz, 2H), 7.99 (d, J = 8.2 Hz, 2H), 7.53 (d, J = 6.0 Hz, 2H), 7.38 (d, J = 4.9 Hz, 4H), 7.18 (d, J = 8.1 Hz, 2H), 4.10 (s, 2H), 3.69 (s, 4H), 2.61 (d, J = 51.7 Hz, 6H), 1.93 (s, 6H), 1.79 (s, 2H), 1.69 (d, J = 11.7 Hz, 8H). ^{13}C NMR (101 MHz, DMSO-d_6) δ 168.45 (s), 166.86 (s), 160.89 (s), 153.34 (s), 151.04 (s), 149.38 (s), 147.20 (d, J = 224.8 Hz), 138.57 (s), 136.98 (d, J = 36.4 Hz), 136.74–136.33 (m), 132.24 (s), 131.10 (s), 130.00 (s), 128.69 (s), 127.60 (dd, J = 64.7, 35.9 Hz), 126.90–126.53 (m), 125.92 (s), 125.57 (s), 123.79 (s), 122.25 (s), 115.51 (d, J = 18.2 Hz), 67.92 (s), 65.61 (s), 57.48 (s), 52.98 (s), 26.70 (s), 25.98 (s), 24.96 (s), 21.92 (s). IR (KBr): ν = 2964, 2918, 2847, 1648, 1445, 1383, 1261, 1109, 1007, 824, 1180, 545 cm^{-1}. HRMS (ESI): m/z: calcd for $[M - 2PF_6]^{2+}$ $C_{55}H_{51}N_9O_2Ru$, 485.6612; found: 485.6612.

4.1.6 Synthesis of [Ru(dip)$_2$(MPLP)](PF$_6$)$_2$ (Ru(II)-3). This complex was synthesized in an identical route to that of **Ru(II)-1** with $[Ru(dip)_2Cl_2]\cdot 2H_2O$ in place of $[Ru(dmb)_2Cl_2]\cdot 2H_2O$. Dark red product. Yield: 191.5 mg, 42.3%. ^{1}H NMR (400 MHz, DMSO-d_6) δ 14.21 (s, 1H), 9.06 (d, J = 8.1 Hz, 2H), 8.36 (d, J = 5.5 Hz, 2H), 8.27 (d, J = 7.2 Hz, 6H), 8.22 (d, J = 5.5 Hz, 2H), 8.08 (s, 2H), 7.82 (d, J = 5.5 Hz, 4H), 7.78 (d, J = 5.6 Hz, 2H), 7.72–7.60 (m, 20H), 7.15 (d, J = 7.7 Hz, 2H), 4.09 (t, J = 6.2 Hz, 2H), 3.57 (t, J = 4.4 Hz, 4H), 2.34 (t, J = 6.9 Hz, 6H), 1.84–1.74 (m, 2H), 1.62 (d, J = 7.3 Hz, 2H). ^{13}C NMR (101 MHz, DMSO-d_6) δ 160.44 (s), 155.08 (s), 152.75 (d, J = 36.5 Hz), 149.88 (s), 148.91–147.93 (m), 145.30

(s), 135.96 (d, $J = 4.8$ Hz), 130.86 (s), 130.70–129.95 (m), 129.95–129.91 (m), 129.58 (s), 129.09–127.68 (m), 126.98 (s), 126.66–125.48 (m), 124.09 (d, $J = 50.3$ Hz), 123.82–123.18 (m), 115.30 (s), 68.03 (d, $J = 12.9$ Hz), 66.73 (s), 58.27 (s), 53.80 (s), 27.05 (s), 22.85 (s). IR (KBr): $\nu = 2959, 2923, 2842, 1607, 1470, 1551, 1454, 1414, 1251, 1104, 1028, 835, 758, 733, 702, 565, 555\ cm^{-1}$. HRMS (ESI): *m*/*z*: calcd for $[M - 2PF_6]^{2+}$ $C_{75}H_{59}N_9O_2Ru$, 609.6928; found: 609.6924.

4.2 Biological activity test

4.2.1 Biological MIC. *S. aureus* strains were cultured to the logarithmic phase and then diluted 1000 times with a fresh TSB medium to obtain a bacterial suspension. Add 50 μL drug and 200 μL bacterial suspension into a 96-well plate. Incubate the plate at 37 °C for 20 h to determine the MIC.

4.2.2 Growth curves of *S. aureus*. *S. aureus* at the logarithmic phase was diluted 100 times with a fresh TSB medium and then transferred into a 24-well plate. Bacterial suspensions were incubated at 37 °C in a plate reader with orbital shaking at 220 rpm. At that time, the absorbance value of 600 nm was measured every 30 min.

4.2.3 Time–kill curve. *S. aureus* at the logarithmic phase was diluted 1000 times with a fresh TSB medium. Then, the bacteria and drugs were mixed and then added into a 24-well plate. After incubating in a shaking table at 37 °C for 6 h, 100 μL diluted solution was plated on a TSB agar plate. The plate was cultured in an incubator at 37 °C, and the number of viable bacteria was counted.

4.2.4 Drug resistance assay. The MIC of the tested drug was determined according to the above method. Then, the bacteria from the 0.5 MIC well were cultured to the logarithmic phase, and then further employed to determine the MIC value of the tested drug again. The above step was repeated 20 times and the changes in MIC values were recorded.

4.2.5 Hemolytic toxin inhibition assay. *S. aureus* at the logarithmic phase was diluted by 1000 times using a fresh TSB medium. Afterward, *S. aureus* was co-incubated with different concentrations of **Ru(II)-3** at 37 °C for 12 h; then, the supernatant was collected by centrifugation (5000 rpm, 5 min). Next, fresh rabbit red blood cells were washed three times with sterile PBS. Then, 50 μL rabbit blood cells and 150 μL bacterial supernatant were added into 1 mL PBS buffer solution, incubated at 37 °C for 30 min, centrifuged, and the supernatant was collected. The hemolytic activity was measured by the absorbance at 543 nm.

4.2.6 Checkerboard assay. At first, the MIC of the selected antibiotics was determined. The overnight-cultured *S. aureus* was diluted 1000-fold with fresh TSB. Then, 25 μL of gradient concentrations of **Ru(II)-3**, 25 μL of gradient concentrations of antibiotics, and 200 μL of diluted bacterial suspension were mixed in a 96-well plate, followed by incubation at 37 °C for 20 h. FICI is defined as the sum of the MIC of each drug when used in combination divided by the MIC of the drug when used alone.

4.2.7 Nucleic acid leakage. To verify membrane damage, the overnight-cultured bacteria were diluted 1 : 1000 in fresh TSB and cultured to the logarithmic phase. Then, the supernatant was removed by centrifugation, and the bacteria were resuspended in PBS to $OD_{600} = 1$. After co-incubating with **Ru(II)-3** or polymyxin B sulfate for 2 h, the ultraviolet absorption (260 nm) of the bacterial supernatant was measured.

4.2.8 Biofilm inhibition and eradication assay. To explore the inhibited effect of **Ru(II)-3** on biofilm formation, *S. aureus* was diluted by 1000 times with TSB and then co-incubated with **Ru(II)-3** in 24-well plates at 37 °C for 48 h. Then, the floating bacteria were removed and washed three times by PBS. After adding 5% crystal violet and incubating for 30 min, excess crystal violet was washed off with sterile water. Afterward, a mixture of acetic acid and water (v/v = 1 : 1) was added and the absorbance at 595 nm was measured. For the biofilm eradication assay, *S. aureus* was cultured in 24-well plates at 37 °C for 48 h to induce the formation of a biofilm; then, the mature biofilm was co-incubated with **Ru(II)-3** for 24 h. Afterward, the biofilm was washed and fresh TSB containing MTT was added. At last, DMSO was added and the UV absorption at 595 nm was measured.

4.2.9 $DiSC_3(5)$ and DAPI/PI dyeing. *S. aureus* at the logarithmic phase was diluted with sterile PBS to $OD_{600} = 0.3$ and then co-incubated with **Ru(II)-3** or vancomycin at 37 °C for 2 h. The resulting bacteria were collected and then washed three times with PBS. The obtained bacteria were resuspended in 5 mL PBS. Afterward, adding 20 μL $DiSC_3(5)$ (30 μM) and incubated for 1 h under dark conditions. For DAPI/PI dyeing, 30 μL DAPI (30 μM) was added into the bacterial suspension (500 μL) and incubated in the dark for 15 min, followed by 30 μL of PI (30 μM) for a further 15 min of incubation. At last, the bacteria-contained films were prepared and photographed with a confocal laser scanning microscope.

4.2.10 DCFH-DA dyeing assay. *S. aureus* at the logarithmic phase was diluted with sterile PBS to $OD_{600} = 0.3$ and then incubated with **Ru(II)-3** at 37 °C for 2 h. The resulting bacteria were collected and then washed three times with PBS; the obtained bacteria were resuspended in 5 mL PBS again. Afterward, 30 μL DCFH-DA (10 μM) was added into the bacterial suspension (500 μL) and incubated in the dark for 30 min. At last, the bacteria-contained films were prepared and photographed with a confocal laser scanning microscope.

4.2.11 *G. mellonella* infection model. *S. aureus* at the logarithmic phase was collected and washed with PBS three times. Next, bacterial cells were diluted with PBS to $OD_{600} = 0.3$. Prior to injection, *G. mellonella* was sterilized with ethanol. Then, 5 μL *S. aureus* was injected into *G. mellonella* from the right front foot. After 1 h, **Ru(II)-3** was injected into *G. mellonella* from the left front foot. At last, the survival rate of *G. mellonella* was recorded within 5 days.

4.2.12 Mouse infection model. To minimize the effects of metabolic differences, only female mouse (KM strain, ~6–8 weeks of age, ~20–25 g of weight) were selected for the mouse infection model. In brief, the back hair of mice was removed with a razor and depilatory cream. Then, the back skin of the mouse was cut to a size of 1 cm with scissors. Next, the *S. aureus* at the logarithmic phase was collected and diluted with PBS to $OD_{600} = 1.0$; then, 100 μL bacterial solution was dropped on the

wound. After 12 h, pustules formed at the site of infection. The infected mice were randomly divided into four groups with five mice in each group. Next, ointments containing **Ru(II)-3** (50 or 100 μg mL^{-1}) was evenly smeared on the wounds three times a day. At last, the changes in wounds and body weight of the mice were recorded every 24 h.

Ethical statement

All mouse were purchased from Nanjing Keruisi animal Co., LTD. The animal study was reviewed and approved by Institutional Animal Care and Use Committee of Jiangxi Science & Technology Normal University, and complied with the academic guidelines for the care and use of laboratory animals of China.

Conflicts of interest

The authors have declared that there is no conflict of interest.

Acknowledgements

We gratefully acknowledge the generous support provided by Health Research Project of Hainan Province (Grant No. 22A200010) and Jiangxi Science & Technology Normal University (2021QNBJRC001).

References

1 G. Maddalena, R. Matteo and V. Pierluigi, Antimicrobial resistance in organ transplant recipients, *Infect. Dis. Clin. N. Am.*, 2023, **37**(3), 515–537.
2 X. Jiaqi, F. Weiguo, W. Jiaye, W. Ruichen, Z. Bowen, B. Letao, C. Zhesheng, Y. Hui and S. Leming, Antimicrobial peptides for combating drug-resistant bacterial infections, *Drug Resist. Updates*, 2023, **68**, 100954.
3 W. Haibo, W. Minji, X. Xiaohan, G. Peng, X. Zeling, Z. Qi, L. Hongyan, Y. Aixin, Y. T. K. Richard and S. Hongzhe, Multi-target mode of action of silver against *Staphylococcus aureus* endows it with capability to combat antibiotic resistance, *Nat. Commun.*, 2021, **12**(1), 3331.
4 C. Gordon, B. Justin and O. Michael, Pathogenicity and virulence of *Staphylococcus aureus*, *Virulence*, 2021, **12**(1), 547–569.
5 A. A. Bandar, A. J. Intisar, M. A. Jawhra, M. A. Hussein, G. Bandar, A. Kholod and Y. Y. Nik, Antimicrobial resistance in methicillin-resistant *Staphylococcus aureus*, *Saudi J. Biol. Sci.*, 2023, **30**(4), 103604.
6 C. J. Murray, *et al.*, Global burden of bacterial antimicrobial resistance in 2019: a systematic analysis, *Lancet*, 2022, **399**(10325), 629–655.
7 Antimicrobial resistance in the age of COVID-19, Nat. Microbiol., 2020, **5**, p. 779.
8 T. M. Rawson, D. Ming, R. Ahmad, L. S. P. Moore and A. H. Holmes, Antimicrobial use, drug-resistant infections, and COVID-19, *Nat. Rev. Microbiol.*, 2020, **18**, 409–410.
9 M. A. Tiburcio, A. R. Rocha, R. A. Romano, N. M. Inada, V. S. Bagnato, R. M. Carlos and H. H. Buzzá, In vitro evaluation of the cis-[Ru(phen)2(pPDIp)]$^{2+}$ complex for antimicrobial photodynamic therapy against Sporothrix brasiliensis and Candida albicans, *J. Photochem. Photobiol., B*, 2022, **229**, 112414.
10 F. Angelo, R. Riccardo, T. Solmaz, B. Olivier, A. Philipp, F. Ariane, M. Tim, S. Leone and G. Gilles, Synthesis, characterization, and biological evaluation of new Ru(II) polypyridyl photosensitizers for photodynamic therapy, *J. Med. Chem.*, 2014, **57**(17), 7280–7292.
11 P. Sudhindra, R. Nilmadhab, K. Binoy and P. Priyankar, Construction of homo and heteronuclear Ru(II), Ir(III) and Re(I) complexes for target specific cancer therapy, *Coord. Chem. Rev.*, 2022, **460**, 214462.
12 R. B. Wang, M. Wei, X. R. Wang, Y. S. Chen, Y. S. Xiong, J. X. Cheng, Y. H. Tan, X. W. Liao and J. T. Wang, Synthesis of ruthenium polypyridine complexes with benzyloxyl groups and their antibacterial activities against *Staphylococcus aureus*, *J. Inorg. Biochem.*, 2022, **236**, 111954.
13 L. Jiang, Y. Y. Ma, Y. S. Xiong, Y. H. Tan, X. M. Duan, X. W. Liao and J. T. Wang, Ruthenium polypyridine complexes with triphenylamine groups as antibacterial agents against *Staphylococcus aureus* with membrane-disruptive mechanism, *Front. Chem.*, 2022, **10**, 1035741.
14 C. Y. Zhang, R. J. Yu, L. Q. Wang, H. Y. Huang, M. Q. Xiao, X. M. Duan, J. T. Wang, X. W. Liao and Y. S. Xiong, Synthesis and evaluation of sulfonyl-substituted ruthenium complex as potential antibacterial activity against *Staphylococcus aureus*, *New J. Chem.*, 2022, **46**, 14805–14815.
15 R. B. Wang, X. M. Zhou, J. J. Chen, Y. S. Chen, Y. S. Xiong, X. M. Duan, X. W. Liao and J. T. Wang, Ruthenium polypyridine complexes containing prenyl groups as antibacterial agents against *Staphylococcus aureus* through a membrane-disruption mechanism, *Arch. Pharm.*, 2023, **356**, 2300175.
16 C. Y. Zhang, R. J. Yu, L. Q. Wang, H. Y. Huang, J. T. Wang, X. W. Liao, X. M. Duan and Y. S. Xiong, Design, synthesis, and evaluation of aryl-thioether ruthenium polypyridine complexes: a multi-target antimicrobial agents against gram-positive bacteria, *Eur. J. Med. Chem.*, 2022, **240**, 114562.
17 K. Archana and K. S. Rajesh, Morpholine as ubiquitous pharmacophore in medicinal chemistry: deep insight into the structure-activity relationship (SAR), *Bioorg. Chem.*, 2020, **96**, 103578.
18 L. Elena, C. Lorenzo and T. Andrea, Occurrence of morpholine in central nervous system drug discovery, *ACS Chem. Neurosci.*, 2021, **12**(3), 378–390.
19 C. Rishav, B. Indira, R. Souryadip, P. Kallol, S. K. Tuhin, G. Arnab and M. Arindam, Synthesis, characterization, and cytotoxicity of morpholine-containing ruthenium(II) p-cymene complexes, *Inorg. Chem.*, 2021, **60**(16), 12172–12185.
20 T. Ariadni, X. Dimitrios and P. K. Angeliki, Morpholine as a scaffold in medicinal chemistry: an update on synthetic strategies, *ChemMedChem*, 2020, **15**(5), 392–403.
21 S. Bu, G. Jiang, G. Jiang, J. Liu, X. Lin, J. Shen, Y. Xiong, X. Duan, J. Wang and X. Liao, Antibacterial activity of

ruthenium polypyridyl complexes against *Staphylococcus aureus* and biofilms, *J. Biol. Inorg. Chem.*, 2020, **25**(5), 747–757.

22 M. E. Ivarsson, D. Estelle, H. Corina, H. Samuel, H. Chrismita, F. Jillian, A. Fernando, L. Jun, F. V. Elena, B. Premysl, M. Susan, C. Wang, L. Jean-Christophe and C. Bastien, Small-Molecule allosteric triggers of Clostridium difficile toxin B auto-proteolysis as a therapeutic strategy, *Cell Chem. Biol.*, 2019, **26**, 17–26.

23 D. Hana, A. Véronique, P. Otto and M. B. Jean, Antibiotic adjuvants: make antibiotics great again, *J. Med. Chem.*, 2019, **62**(19), 8665–8681.

24 F. E. Raquel, E. P. Jake, O. W. Jonathan, B. S. Paul and M. E. Richard, Depolarization, bacterial membrane composition, and the antimicrobial action of ceragenins, *Antimicrob. Agents Chemother.*, 2010, **54**(9), 3708–3713.

25 G. Yong, H. Enhua, W. Tingyu, Y. Xiaoting, H. Meiyue, B. Li-Ping, F. Xiangjing, L. Jifeng and Q. Shangshang, Development of Membrane-Active Honokiol/Magnolol Amphiphiles as Potent Antibacterial Agents against Methicillin-Resistant Staphylococcus aureus (MRSA), *J. Med. Chem.*, 2021, **64**, 12903–12916.

26 L. Guo, C. Zhang, G. Chen, M. Wu, W. Liu, C. Ding, Q. Dong, E. Fan and Q. Liu, Reactive oxygen species inhibit biofilm formation of Listeria monocytogenes, *Microb. Pathog.*, 2018, **127**, 183–189.

27 E. Evgeniy and K. Sergei, Identification of ROS using oxidized DCFDA and flow-cytometry, *Methods Mol. Biol.*, 2010, **594**, 57–72.

28 K. M. James, P. S. Joseph, P. B. Benjamin, M. M. Gabriel, M. Andre, H. L. Sophia, K. Hahn, D. R. Joshua, T. Athanasios, M. S. Mikhail, Z. W. Maxwell and G. Zemer, A dual-mechanism antibiotic kills Gram-negative bacteria and avoids drug resistance, *Cell*, 2020, **181**, 1–15.

29 J. J. Hu, N. Liu, Q. Q. Fan, Y. Q. Gu, S. J. Chen, F. Zhu and Y. Y. Cheng, A fluorous peptide amphiphile with potent antimicrobial activity for the treatment of MRSA-induced sepsis and chronic wound infection, *Angew. Chem., Int. Ed.*, 2024, e202403140.